Journal of Photochemistry and Photobiology A: Chemistry 269 (2013) 34–41

Contents lists available at ScienceDirect

Journal of Photochemistry and Photobiology A: Chemistry

journal homepage: www.elsevier.com/locate/jphotochem

Plasmonic enhancement of photodynamic cancer therapy

Steven C. Hayden[a,1], Lauren A. Austin[a,1], Rachel D. Near[a], Ramazan Ozturk[b], Mostafa A. El-Sayed[a,*]

[a] Laser Dynamics Laboratory, School of Chemistry and Biochemistry, Georgia Institute of Technology, Atlanta, GA 30332-0400, United States
[b] Department of Chemistry, Faculty of Arts and Science, Fatih University, Istanbul 34500, Turkey

ARTICLE INFO

Article history:
Received 25 September 2012
Received in revised form 4 June 2013
Accepted 7 June 2013
Available online 21 June 2013

Keywords:
Nanoparticle
Photodynamic cancer therapy
Surface plasmon resonance
Singlet oxygen

ABSTRACT

Photodynamic therapy combines light, oxygen, and a photosensitizer (PS) to excite molecular oxygen to a highly cytotoxic electronic state. We demonstrate two orders of magnitude enhancement of the *in vitro* efficacy of a model PS drug, protoporphyrin IX (PpIX), using nanoparticles (NPs) to plasmonically enhance the photo processes involved in PS anticancer activity. The role of plasmonic enhancement is investigated by controlling the energetic overlap of the plasmon resonance with PpIX absorption using silver nanospheres, gold nanospheres, and gold nanorods. All NP-PpIX complexes, including silver nanospheres, are shown to be non-toxic in the dark due to the lack of cellular endocytosis. This NP delivery system illustrates an important application of nanotechnology to medicine, providing for reduced drug doses, reduced systemic toxicity, and reduction in the amount of time the patient must spend in the dark following treatment.

1. Background

Photodynamic therapy (PDT), in which light and molecular photosensitizers (PS) are used to treat cancers, has come to the forefront of cancer therapeutic options. This type of therapy offers a minimally invasive alternative to procedures such as surgery [1], making it ideal [2] and currently prevalent [3] for cancers of the skin, head, and neck. The technique exploits photosensitizer (PS) drugs that are capable of producing singlet oxygen ($^1O_2$) [4], which is highly reactive and thus highly destructive in a cellular environment. Further, the short diffusion pathlength of $^1O_2$ is an applicative boon for PDT, as it confines the region of treatment [5]. Photosensitizer drugs also show a low incidence of dark toxicity [1,3].

Successful administration of PDT requires only oxygen, the PS molecule, and light of an appropriate wavelength to excite the PS [6]. The drug selection and excitation wavelength is dictated by the therapeutic window (~600–1200 nm), which results from the high extinction of human tissue for blue and green light and relatively weak extinction for red light [7]. Thus, blue light absorbers are useful for epithelial-depth and post-surgical PDT [1,3,8], and NIR absorbers are useful for deep tissue and solid tumor PDT [9–11]. While porphyrin and phthalocyanine PDT drugs exhibit high $^1O_2$ quantum yields, these large macrocycles suffer from inherent hydrophobia [12]. This hydrophobia is a major limitation to the circulation half-lives and activities of these drugs [13], as they aggregate relatively quickly in biological serum [11]. Yet another limitation to the use of these drugs is their dependence on passive targeting; when administered systemically, they accumulate in tumors merely due to the enlarged vasculature and lack of lymphatic drainage therein [10].

Due to the reliance of PS drugs on passive targeting, significant attention has been given to PDT drug administration platforms. Metal nanoparticles (NPs), in particular, have been used to extend the circulating half-lives of PDT drugs in serum [14] and selectively deliver drugs to tumor tissue through ligand targeting [15]. Much less attention has been given to the use of NPs beyond regio-specific drug transport vectors. However, plasmonic metal NPs also possess the ability to increase the absorption cross section – and therefore anticarcinogenic activity – of photosensitizer drugs [16].

Plasmonic particles are unparalleled in their ability to harvest light energy [17,18]. The constructive use of this light-harvesting ability to enhance radiative processes in adjacent systems (e.g. photosensitizers) is strongly dependent on the particles' characteristics (e.g. size, shape, composition), as these determine the optical properties of the nanoparticle [19]. Energetic overlap between plasmon resonance and PS absorption increases PS activity, whereas plasmon overlap with PS emission will quench its activity [20–22]. Very recently, Oo et al. examined a system employing gold nanospheres and protoporphyrin IX (PpIX) [23], in which the plasmon resonance overlapped partially with the PS absorbance and not with its emission; an increase in singlet oxygen generation

* Corresponding author. Tel.: +1 404 894 0292; fax: +1 404 894 7452.
E-mail address: melsayed@gatech.edu (M.A. El-Sayed).
[1] Equal contribution authors.

1010-6030/$ – see front matter © 2013 Elsevier B.V. All rights reserved.
http://dx.doi.org/10.1016/j.jphotochem.2013.06.004

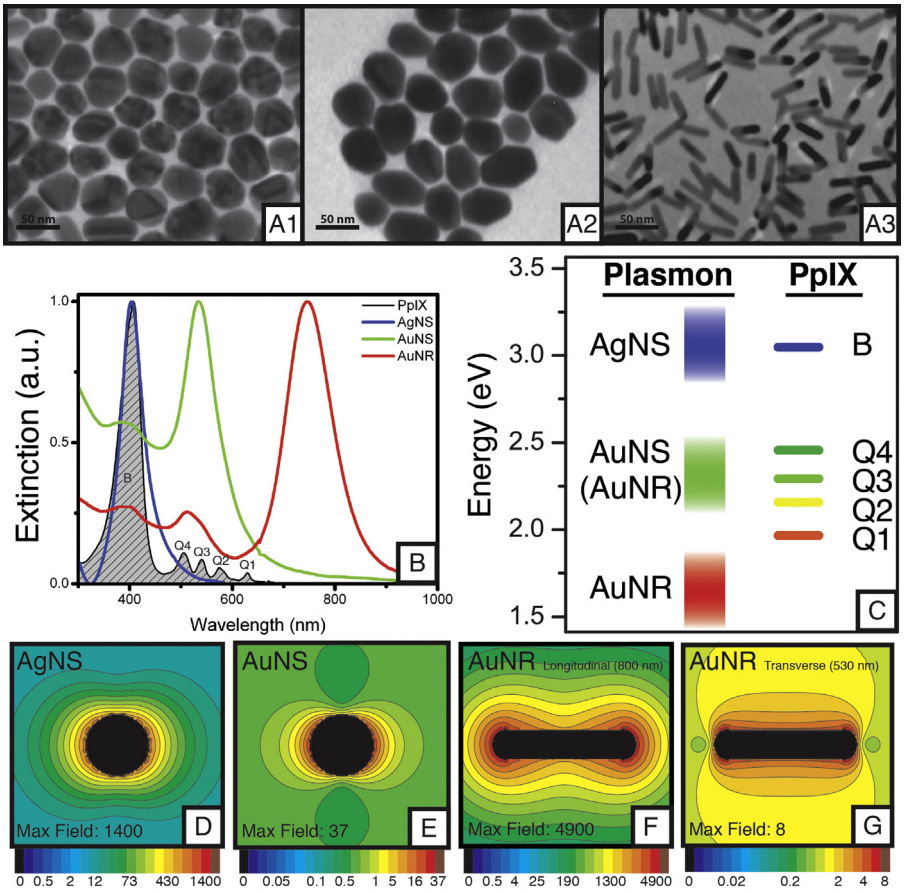

Fig. 1. NP and PpIX physical and energetic characteristics. TEM micrographs of (A1) AgNS, (A2) AuNS, (A3) AuNR. (B) Extinction spectrum of PpIX (shaded gray), AgNS (blue), AuNS (green), and AuNR (red). (C) Jablonski diagram of plasmon resonances for each particle and the Q and B excitation bands of PpIX, illustrating the overlap between the various plasmon resonances and these PpIX excitation energies. Note that the energy of the transverse plasmon mode arising in AuR gives this resonance a degree of overlap with the Q band excitation energies similar to but weaker than that seen in AuS. (D–G): Discrete dipole approximation electric field plots for (D) AgNS at 412 nm, (E) AuNS at 530 nm, and AuNR for both the (F) longitudinal plasmon mode at 800 nm and (G) the transverse plasmon mode at 530 nm. Maximum field strengths are indicated for each resonance.

(SOG) was observed with increasing plasmon strength, as the larger particles with stronger plasmon field better intensify the absorption of adjacent drug molecules.

Absorption of light by a metal nanoparticle occurs either by excitation of *d* orbital transitions, called the inter-band transitions, or through interaction with the plasmon resonance. Absorption by the interband invariably results in thermal or other non-radiative relaxations and is thus non-advantageous in a NP–PS system. Interband transitions are a property of the metal; they cannot be adjusted by changing particle size or shape. All gold nanoparticles will therefore show some degree of competitive filtering of UV to green light, as their interband transitions are in this region, whereas silver interband transitions are in the UV. Excitation of the plasmon, on the other hand, should increase the absorption – and therefore emission and SOG – of photosensitizers on the particle surface, given spectral overlap between the plasmon and the PS absorption. The ability to tune the plasmonic resonance of nanoparticles throughout the visible energy spectrum is a defining and highly important characteristic of these systems and is an area our lab has explored in depth [18,19,24–28]. Given that plasmon resonance results in such a strong interaction with incident photons, it follows that proper manipulation of the plasmon energy will allow for unparalled enhancement of photosensitizers within the NP plasmonic field [16,22,29].

Herein, we systematically examine the role of overlap between the energy of the plasmon and the absorption and emission of a model porphyrin photosensitizer (Protoporphyrin IX, PpIX) using silver nanospheres (AgNS, 40 nm diameter), gold nanospheres (AuNS, 40 nm diameter), and gold nanorods (AuNR, 40 nm length, 10 nm width). The combination of these systems provides a cohesive survey of plasmonic enhancement, competitive filtering, and emission quenching of this model PS by these characteristic plasmonic nanoparticles. In addition, we vary the nature of PpIX association with the particle surface to contrast the unloading ability provided by electrostatic complexes with the plasmonic effect on PpIX activity using rigid surface attachment. Further, we vary the distance between the porphyrin and the particle surface in our covalently-attached complexes to judge the effect of non-radiative energy transfer processes and plasmonic field strength for each of our three nanoparticle types.

2. Materials and methods

2.1. Reagents

Silver nitrate (7761-88-8), sodium citrate (6132-0403), sodium borohydride (16940-66-2), cetyl-trimethylammonium bromide (CTAB, 57-09-0), hydrogen tetrachloroaurate trihydrate ($AuCl_4$, 16961-25-4), dimethyl sulfoxide (DMSO, 67-68-5), and 9,10-Anthracenediyl-bis(methylene)dimalonic acid (ABDA, 307554-62-7) were obtained from Sigma Aldrich, St. Louis, MO. Ascorbic acid (AA, 50-81-7) was obtained from Mallinckrodt, Phillipsburg, NJ. All chemicals were used as received.

2.2. AgNS Synthesis

For the preparation of silver nanospheres (40 nm diameter), $AgNO_3$ (25 mL, 1 wt%) was added to boiling water (deionized, 175 mL) in a covered, trace-clean, 250 mL Erlenmeyer flask at a stir speed of 500 rpm. At reboil, the watch glass cover was removed, and citrate solution (8 mL, 38.8 mM) was added to the flask. The stir speed was increased to 1000 rpm, and sodium borohydride (2.4 mL, 0.1 M) was injected quickly and all at once. The stir speed was then reduced to 500 rpm as the solution turned black. The heat was turned off, and the solution was allowed to stir for 5 min. The resulting creamy, light-green solution was covered and placed in the dark overnight to allow the particles to ripen. The particles were then characterized by UV–vis (Ocean Optics HR4000CG-UV-NIR) and TEM.

2.3. AuNS Synthesis

Gold nanospheres (40 nm diameter) were synthesized using a modified seed-mediated gold nanorod synthesis [30]. The seed solution was first prepared by dissolving CTAB (0.273 g) in water (deionized, 7.5 mL) with mild stirring and slight heating. Hydrogen tetrachloroaurate trihydrate (250 μL, 10 mM) was added, and then the gold was reduced with sodium borohydride (600 μL, 0.1 M). The solution was stirred for 5 min before use. The growth solution was prepared by dissolving CTAB (15.49 g) in water (deionized, 425 mL) with mild stirring and slight heating. Tetrachloroaurate trihydrate (20 mL, 10 mM) was then added, yielding a clear, bronze-colored solution. The gold was then reduced with ascorbic acid (11.6 mL, 79 mM), yielding a clear, colorless solution. The seed solution (350 μL) was then injected, and the solution was stirred (400 rpm) for 3 h.

2.4. AuNR synthesis

Gold nanorods (10 nm diameter, 40 nm length) were synthesized using a seed-mediated approach [30]. The seed solution was first prepared by dissolving cetyl-trimethylammonium bromide (CTAB, 0.273 g) in water (deionized, 7.5 mL) with mild stirring and slight heating. Hydrogen tetrachloroaurate trihydrate (250 μL, 10 mM) was added, and the gold was reduced with sodium borohydride (600 μL, 0.1 M). The solution was stirred for 5 min before use. The growth solution was prepared by dissolving CTAB (15.49 g) in water (deionized 425 mL) with mild stirring and slight heating. Tetrachloroaurate trihydrate (20 mL, 10 mM) was then added, yielding a clear, bronze-colored solution. Silver nitrate (8.5 mL, 4 mM) was added, and then the gold was reduced with ascorbic acid (11.6 mL, 79 mM), yielding a clear, colorless solution. Seed solution (960 μL) was injected, and the solution was left undisturbed.

2.5. NP-PpIX complex synthesis

Clean AgNS, AuNS, and AuNR were combined with unmodified PpIX, Short-Linker PpIX, and Long-Linker PpIX to generate solutions of 0.1 nM NPs and 0.2 and 2.0 μM PpIX. Polyethylene glycol with methoxy and thiol terminii (mPEG-SH) was added to provide approximately 10% NP surface coverage in order to maintain good water solubility and improve biocompatibility. Final DMSO concentration was maintained at 0.2%, and this amount of DMSO showed no effect on cell viability by itself. NP-PpIX complexes were characterized using UV-Vis, TEM, and Dynamic Light Scattering (DLS).

2.6. Transmission electron microscopy (TEM)

The vertical drying method was used to deposit nanoparticles onto carbon-coated copper TEM grids, which were then screened at a magnification of 100,000× using a Jeol 100-CX TEM operated at an acceleration voltage of 100 kV and equipped with a CCD camera.

2.7. Discrete dipole approximation (DDA)

The optical responses of the various nanoparticles were calculated using the DDA method with the DDSCAT 6.1 code offered publicly by Draine and Flatau [31]. The bulk values of the dielectric constants for gold and silver reported by Johnson and Christy [32] were used, and the medium was assumed to have a refractive index of 1.33 corresponding to that of liquid water. Additionally, the surface field intensities around the particles were calculated using a modified version of the DDSCAT code provided by the Schatz group [33,34].

2.8. Singlet oxygen measurements

The relative rate of singlet oxygen generation (SOG) in solution was measured for each complex and for PpIX alone using a scavenger (9,10-Anthracenediyl-bis(methylene)dimalonic acid, ABDA). ABDA (1.5 mL, 0.2 mM) was combined with water (deionized, 1 mL) and sample (1 mL) and then split into two cuvettes. One was placed in the dark to serve as the reference cuvette, and one was irradiated using a Xe arc lamp (1 W) fitted with a water filter to block IR (heat) and a long-pass filter (450 nm) to block UV and prevent photobleaching of the ABDA itself. The absorbance of both the sample and reference cuvettes was collected periodically over 500 s, and the disappearance of the ABDA bands was monitored, plotted as a function of time, and fit with a curve. The relative rate constants of SOG were calculated from the slope of this decay curve.

2.9. Dynamic light scattering

DLS measurements were taken using a NanoZS Zetasizer particle analyzer (Malvern, 633 nm).

2.10. Cell culture

Human oral squamous carcinoma cells (HSC-3), a malignant epithelial cell line, were cultured in Dulbecco's Modified Eagle's Medium (DMEM) (Mediatech) supplemented with 4.5 g/L glucose, sodium pyruvate, 10% v/v fetal bovine serum (FBS) (Mediatech) and 1% antimycotic solution (Mediatech). Cell cultures were kept at 37 °C in a 5% CO_2 humidified incubator.

2.11. Cell PDT complex treatment and light exposure

HSC-3 cells were grown in 96 well plates for 24 h and then incubated with the respective NP-PpIX complexes in culture medium (DMEM) for 24 h. Each nanoparticle concentration was kept constant at 0.1 nM, while PpIX concentrations were varied from 0.0–20.0 μM. Cells were then irradiated (10 mW, 30 min) with a Xe arc lamp fitted with a short-pass water filter (heat), a long-pass UV filter (350 nm), a 90° turning mirror, and a 30° light diffuser to ensure equal intensity for every well. Control cells were removed from the incubator along with the sample cells and placed in the dark. Nanoparticles and PpIX were removed and ∼25% XTT reagent (Sigma) in culture medium (DMEM) was added. Cells were kept at 37 °C in a 5% CO_2 humidified incubator for ∼5 h-overnight. Absorbance measurements at 450 nm and 690 nm were taken on a Biotek Synergy H4 Multi-Mode Plate Reader.

2.12. Dark field imaging

Cells were cultured on 18 mm diameter glass coverslips for 24 h and incubated with the respective NP-PpIX complexes diluted in

culture medium (DMEM) for 24 h. The nanoparticle and PpIX concentrations were kept constant at 0.1 nM and 0.2 μM, respectively. Particle solutions were removed and coverslips were then washed with DPBS buffer and fixed with 4% paraformaldehyde. Images were obtained with an inverted Olympus IX70 microscope with a dark field condenser (U-DCW). A 100×/1.35 Iris objective (UPLANAPO) was utilized to collect the scattered light from the NP treated samples.

2.13. Data and statistical analysis

Nanoparticle histograms and average dimensions were obtained via measurement of at least 250 particles for each particle type using ImageJ software. Fluorescence, SOG, DLS, and cell viability data analysis was conducted using OriginLab 8.5. Results are reported as mean ± SD of three or more independent experiments. Cell viability data was analyzed using the *t*-test calculator (GraphPad Software, GraphPad Software, Inc.) and statistical significance was determined from PpIX treated cells to NP-PpIX complex treated cells unless otherwise noted. Data was considered statistically significant if the *P* value < 0.05.

3. Results and discussion

3.1. Nanoparticle selection: Achieving maximum spectral overlap between plasmon resonance and drug absorption

Three types of plasmonic nanoparticles were chosen to investigate the effect of these on singlet oxygen generation (SOG) and cancer cell death by protoporphyrin IX (PpIX): AgNS, AuNS, and AuNR (Fig. 1A, S1 and S2). We maintained similar hydrodynamic radii (Fig. S3) to minimize error from differences in cellular uptake. Plasmon resonance interacts constructively to yield an increase in PpIX absorption, given proper spectral overlap between the plasmon resonance and the PpIX absorbance. AgNS have a strong plasmon resonance (Fig. 1D) in the blue wavelength region (~400 nm) where the Soret band absorbance of the PpIX lies (Fig. 1B and C, blue). The interband transitions of silver are in the ultraviolet and are therefore moot in this visible-light system. These AgNS particles should therefore show the strongest enhancement of PpIX absorption with no competitive filtering by *d–d* transitions. The gold interband, however, absorbs from the UV into the green spectral region and will thus function as a competitive filter of the incident excitation energy in this region. AuNS possess a plasmon resonance that overlaps with the Q band absorptions in PpIX (~530 nm, Fig. 1B and C, green). This resonance is weaker in intensity than that seen in AgNS (Fig. 1E) but will still lead to enhancement of said absorptions. Excitation of these transitions also results in emission and singlet oxygen production, though the emission is correspondingly weaker (Fig. S4).

Gold nanorods have a strong longitudinal plasmon resonance in the therapeutic window (~800 nm, Fig. 1B, C, red, Fig. 1F). However, the emission of most photosensitizers is also in this region, and this leads to quenching of the emission and SOG of bound photosensitizers [35]. AuNR also show a very weak surface plasmon resonance in the green, corresponding to the excitation of their transverse plasmon mode (~530 nm, Fig. 1G); the energy of this oscillation will provide some enhancement of PS molecules along the sides of the rod.

In summary, we observe: (1) plasmonic enhancement of PpIX absorption for AgNS-PpIX complexes; (2) competitive interband filtering of PpIX Soret band excitation energy and plasmonic enhancement of PpIX absorption in the case of AuNS-PpIX complexes; and (3) interband filtering, plasmonic enhancement of PpIX absorption, and emission quenching in the case of AuNR-PpIX complexes. All of these complexes have the advantage that they will increase the solubility of PpIX in biological media. Each of these was prepared at a constant concentration of NPs and varied concentrations of PpIX.

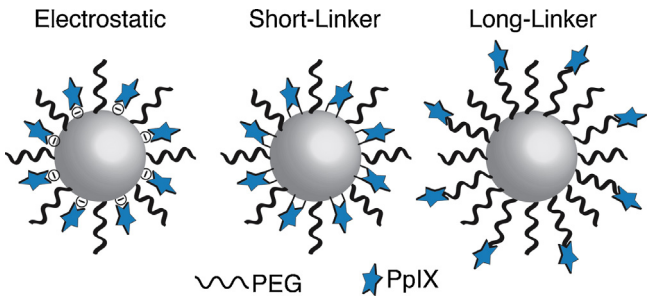

Fig. 2. Schematic diagram of NP complexes with PpIX (blue star) showing the three conjugation methods used. PEG is represented in black. (For interpretation of the references to colour in this figure legend, the reader is referred to the web version of this article.)

3.2. Modification of protoporphyrin IX allows for incorporation into three different plasmonically enhanced complexes for each NP

PpIX is easily modified through a series of peptide bond couplings to generate thiol-functionalized derivatives of the drug without compromising its spectral characteristics or photodynamic activity (see Materials and Methods). The addition of this thiol modality allows for the facile, stable attachment of PpIX to a gold or silver nanoparticle surface due to the relatively strong nature of gold–thiol and silver–thiol bonds. We first examined the unmodified PpIX in an electrostatic complex with NPs. In the second case, we modified PpIX with a peptide bond to yield Short-Linker PpIX with a thiol terminus (Fig. S5). In the third, we functionalized PpIX with a PEG-thiol to generate Long-Linker PpIX, with a larger distance between the fluorophore and the NP surface (Fig. S6). Fig. 1B shows the spectral extinction characteristics of stable complexes between PpIX (gray) and AgNS (blue), AuNS (green), and AuNR (red), and schematic renderings of these are presented in Fig. 2.

3.3. Cell viability studies demonstrate that enhanced photoexcitation allows for the use of 200 times less drug

In our studies with human oral squamous carcinoma cells (HSC-3), PpIX began to show some cytotoxic effect at a concentration of around 20 μM (Fig. 3, black), yielding approximately 30% cell death at this concentration. We treated cells with AgNS, AuNS, and AuNR particle conjugates using NP and PpIX concentrations that caused negligible cell death in cells treated with NP or PpIX alone (0.1 nM and 0.2 μM, respectively, data in Figs. S7–9). Under the same exposure conditions, Short-Linker AgNS-PpIX show cytotoxicity at as low as 0.2 μM – a factor of 200 less drug than PpIX alone – and yield significantly higher cell death at this concentration (60% cell death, Fig. 3B, blue). Short-Linker AuNS complexes show activity at 2 μM (Fig. 3, green), still an order of magnitude lower than the free drug. It is of note here that the AgNS-PEG particles with no porphyrin do not cause any statistically significant cell death on their own at the concentration used here (Fig. S7). This is likely due to the lack of NP internalization under these conditions, which we explore in the next section

We observed decreased activity for the Electrostatic NP-PpIX complexes relative to the Short-Linker complexes, which corroborates the *in situ* results presented forthwith. Electrostatic AgNS-PpIX showed ca. 12% less activity compared to their Short-Linker counterparts, whereas Electrostatic AuNS-PpIX showed negligible activity versus Short-Linker AuNS-PpIX. This is a result

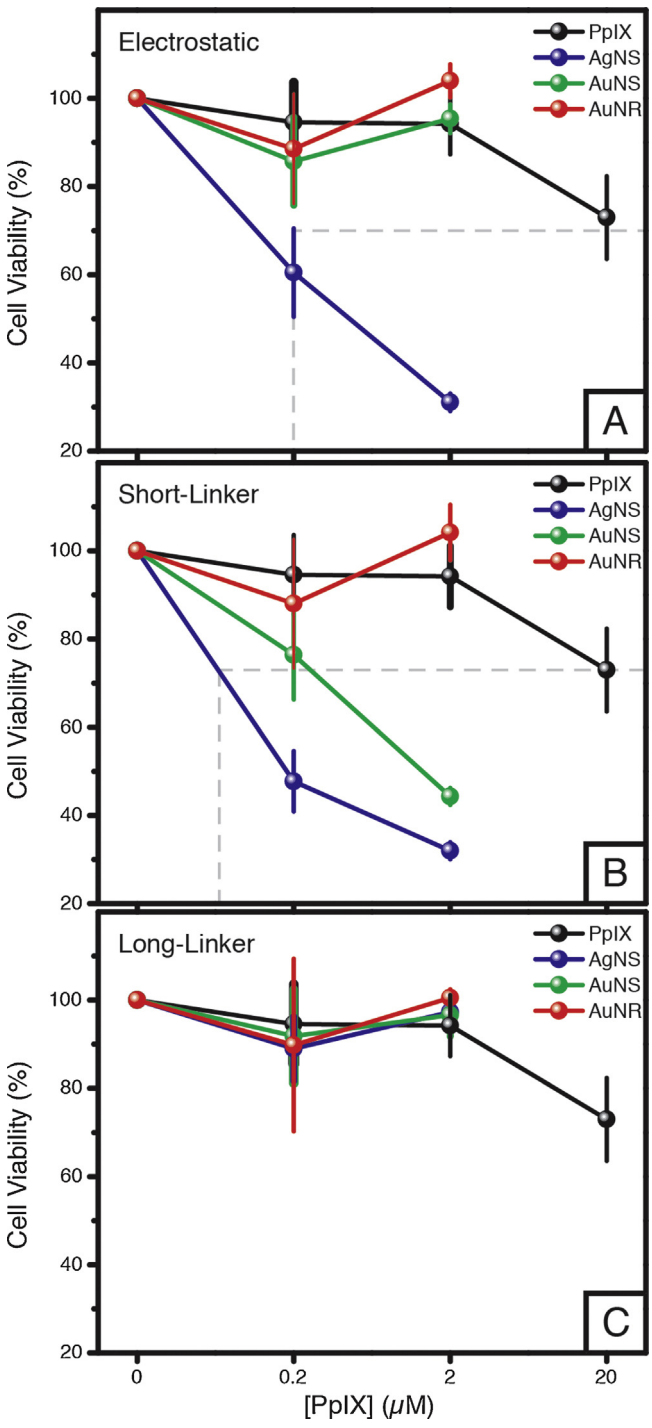

Fig. 3. Cell viability data of HSC-3 cancer cells treated with free PpIX (black) and PpIX conjugated via (A) Electrostatic, (B) Short-Linker, and (C) Long-Linker to AgNS (blue), AuNS (green), and AuNR (red). Short-Linker AgNS-PpIX show a statistically significant decrease in cell viability at only 0.2 μM PpIX. Short-Linker AuNS-PpIX show a statistically significant decrease in cell viability at 2 μM PpIX. AuNR-PpIX shows no statistically significant change in cell viability when compared to PpIX alone at these concentrations. Error bars indicate ± one standard deviation of three independent experiments with p-value < 0.05.

of unloading of the drug from the NP surface during the 24-h incubation period of cells with the complexes [14,35], as ions in the biological medium destabilize the electrostatic association between PS and NP. This effect is more pronounced in gold complexes versus silver because PpIX is electrostatically coordinated to the NP surface through its carboxylic acid groups, and the strength

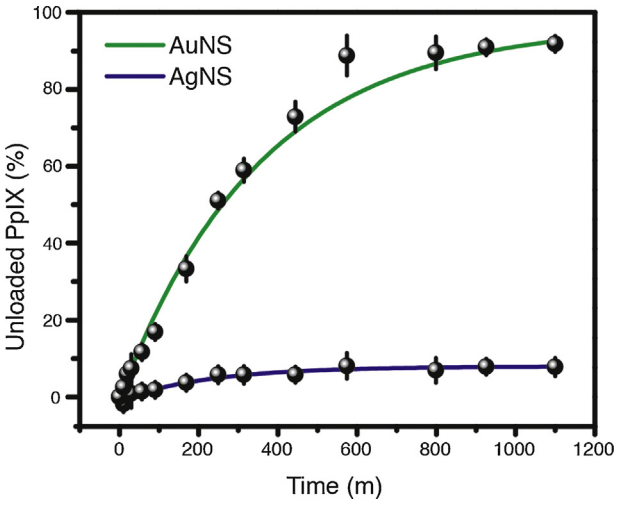

Fig. 4. Diffusion of PpIX drug from AgNS-PpIX (blue) and AuNS-PpIX (green) Electrostatic complexes in water into toluene over time. AuNS-PpIX Electrostatic complexes unload ca. 95% of the drug after 24 h, whereas AgNS-PpIX complexes unload only ca. 10% of the PpIX coordinated to the AgNS surface. This illustrates the relative strength of the silver-carboxyl interaction relative to the gold-carboxl interaction and explains why AgNS-PpIX Electrostatic complexes show similar activity to AgNS-PpIX Short-Linker complexes – with the majority of the drug left on the AgNS surface, plasmonic enhancement of drug activity still occurs. (For interpretation of the references to colour in this figure legend, the reader is referred to the web version of this article.)

of metal–carboxylic acid interaction is stronger for silver than for gold [36,37]. Thus, PpIX unloads more readily from gold than from silver, and the Electrostatic AgNS-PpIX complexes retain more plasmonic enhancement and cause more cell death from residual drug left on the NP surface relative to Electrostatic AuNS-PpIX complexes. *In situ* experiments monitoring the diffusion of PpIX drug from Electrostatic NP-PpIX complexes in water into toluene [14] confirm that almost all of the drug is unloaded from the gold surface compared to only ca. 10% unloaded from silver (Fig. 4).

Toxicity was not observed for Long-Linker NP-PpIX complexes (Fig. 3C) due to the decreased plasmon field strength away from the NP surface. In all of these experiments, we observed a leveling-off of cell death percentage even with further increased concentrations of PpIX. We attribute this to an exhaustion of the available oxygen in the cell medium under these conditions, an issue that could be easily resolved in a clinical setting by maintaining an oxygen flow over the treatment area.

3.4. NP-PpIX complexes remain in the extracellular environment; AgNS-PpIX show surprising lack of dark toxicity

Without a ligand that triggers endocytosis, these NP-PpIX complexes remain in the extracellular environment. This is likely due to their size – ~60–70 nm hydrodynamic diameter (Fig. S3). Dark field analysis of cells following 24 h incubation with our NP-PpIX complexes shows negligible internalization of the particles (Fig. 5), suggesting that cell death is induced by cell membrane damage [38]. Furthermore, HSC-3 human oral squamous carcinoma cells display morphological signs of apoptosis following treatment with light and our NP-PpIX complexes; visible cell shrinkage is apparent when compared to cells exposed only to PEG-conjugated NPs.

3.5. Direct measurement of singlet oxygen provides in situ quantification of photodynamic potential

Singlet oxygen generation was measured using a scavenger molecule, 9,10-Anthracenediyl-bis(methylene)dimalonic acid (ABDA), whose absorbance shifts from the visible to the UV

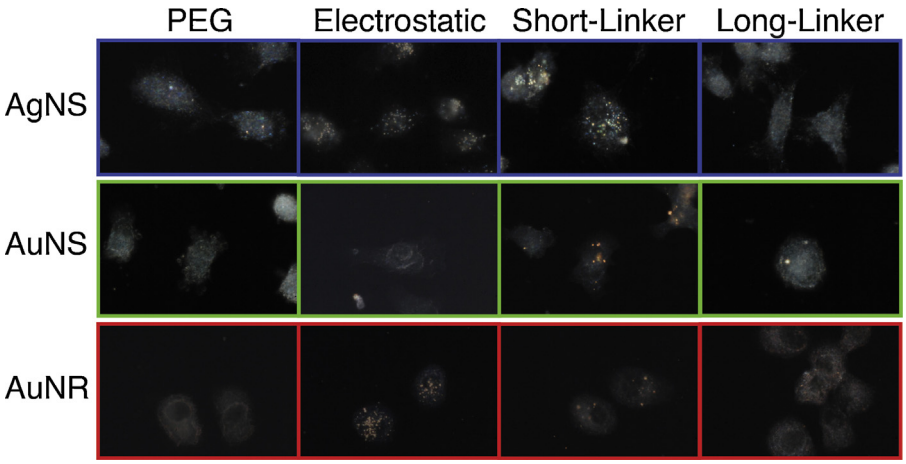

Fig. 5. Dark field microscopy images of HSC-3 cells after 24 h of incubation with NP-PpIX complexes. All NP-PpIX conjugates and PEG-NPs showed minimal uptake, which is indicated by the lack of localized light scattering within the cells. Scale bars represent 10 μM. (For interpretation of the references to colour in this figure legend, the reader is referred to the web version of this article.)

upon reaction with $^1O_2$ (Materials and Methods, Fig. S10). As ABDA photobleaches fairly rapidly when irradiated with light of <420 nm, a long-pass filter was used to block this region of the spectrum (Fig. S11). The inclusion of this filter precludes accurate measurement of SOG rate for AgNS-PpIX complexes, as the plasmon resonance is also in this <420 nm wavelength region. Therefore, SOG rate constants were determined for each modified PpIX alone and for each AuNS-PpIX and AuNR-PpIX complex. All NP-PpIX complexes showed enhanced SOG relative to PpIX alone, with the Short-Linker method of attachment (Fig. 6, green) providing the best enhancement for both AuNS and AuNR.

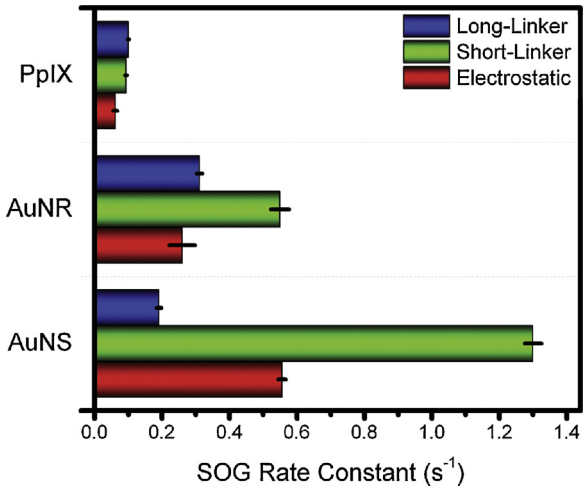

Fig. 6. Singlet oxygen generation rate constants for PpIX, AuNS-PpIX, and AuNR-PpIX under Electrostatic (red), Short-Linker (green), and Long-Linker (red) conjugation. AgNS-PpIX showed comparable activity to free PpIX due to the filter used in this experiment, which keeps the detector molecule from photobleaching but also prevents excitation of the AgNS plasmon. This illustrates the role of plasmon resonance in enhancement. Greater enhancement of SOG is seen in AuNS-PpIX versus AuNR-PpIX for Short-Linker and Electrostatic conjugations. Within each NP group, the greatest enhancement is seen for the Short-Linker complexes, where the PpIX is bound close to the NP surface. Electrostatic complexes show decreased SOG as a result of PpIX unloading from the NP surface during the experiment. Long-Linker AuNS complexes show the least activity due to the distance between the particle surface and the PpIX, as the NP field is weaker out from the NP surface. AuNR-PpIX Long-Linker complexes show greater activity versus AuNS-PpIX Long-Linker due to preferential attachment of the thiol linker to the ends of the rods and the resultant ability of the PpIX to lie along the sides of the rod, where favorable plasmon resonance occurs. Error bars indicate ± one standard deviation of three or more independent experiments.

Electrostatic AuNS-PpIX complexes showed significantly less overall enhancement relative to their Short-Linker counterparts (Fig. 6, red), a likely result of PpIX detachment from the particle surface over the course of the experiment. This illustrates that the increased activity for the electrostatic complexes observed in the cell studies is due largely to vectorial transport of PpIX to the cell membrane by the NP rather than plasmonic enhancement of the porphyrin. This unloading of the drug is advantageous from a solubility standpoint, as the particle helps transport the PpIX close to the cell membrane where the drug sequesters in the lipophilic membrane [1]. However, these delivery and solubility benefits do not outstrip the enhancement effect seen in the Short-Linker complexes, as these maintain plasmonic enhancement of the drug.

Long-Linker AuNS-PpIX complexes showed the least enhancement of SOG relative to the other complexes (Fig. 6), likely due to the increased distance of PpIX from the particle surface and resultant weaker interaction with the plasmon field. Interestingly, Long-Linker AuNR-PpIX complexes showed increased activity relative to AuNS-PpIX particles with the same conjugation. We postulate that this effect arises from the arrangement of this PEG-modified PpIX on the surface of the particle. Thiol groups favor attachment to the crystal surface located at the ends of gold nanorods versus those along the sides [23]. This allows for these PpIX, at the end of a relatively long, malleable polymer chain, to locate preferentially along the sides of the rod, though their thiol tails are attached to the nanorod ends. As illustrated in Fig. 1G, the plasmon band resulting from the transverse plasmon oscillation corresponds to the peak at ~530 nm, and this oscillation would show similar plasmon enhancement of PpIX activity as that seen in gold nanospheres, though its intensity is much weaker than that of a gold nanosphere (Fig. 1E). Thus, slight enhancement of PpIX activity results here from localization of the actual PpIX moiety away from the unfavorable, emission-quenching longitudinal plasmon resonance and closer to the favorable, transverse plasmon oscillation.

4. Conclusions

We found that the strongest enhancement of photosensitizer activity occurs when the drug is covalently bound close to the spherical nanoparticle surface, where the strong plasmon field increases the drug absorption cross-section. Results from *in vitro* experiments show that the amount of drug needed to achieve significant cancer cell death is reduced by two orders of magnitude for silver nanosphere-drug complexes and by one order of magnitude for gold nanosphere-drug complexes. The use of a NP platform

both increases the solubility of the photosensitizer and enhances its quantum efficiency. The NP platform also provides the opportunity to introduce targeting ligands to the system, an advantage that our lab is now exploring. This will greatly increase the specificity of these complexes to target cancerous cells preferentially over healthy cells.

We postulate that the NPs either increase the overall absorption efficiency of PpIX or that the NPs transfer energy to the PS molecules. The NP–PS complex thereby increases the quantum yield of singlet oxygen production by the PS drug. These complexes are not endocytosed by the cell; this allows for the use of silver NPs without the toxicity that has been observed in other studies when silver NPs are endocytosed [39]. This further suggests that the complexes could be removed easily if used for surface treatment. However, should future *in vivo* experiments reveal dark toxicity of silver NP–PS complexes, gold NP-PS complexes, known for their lack of *in vivo* toxicity, could be used instead. This opens the door for the use of other nanoparticle shapes, such as nanocubes, which are known to have stronger fields and may therefore yield even greater enhancement of PS activity. The shape-dependence of this enhancement is now being explored in our lab.

A limitation to the use of these NP complexes in the body arises from the poor tissue penetration depth of the visible light needed to excite these silver or gold nanospheres, which could limit the use of these complexes to surface treatments. Tissue penetration depth in the red is quite high, but NPs with plasmon resonance in the red quench the emission and activity of PS molecules bound to their surface, as this emission is also in the red. Further, the energy required to generate singlet oxygen precludes both direct excitation of molecular oxygen [40] and the use of a drug with an absorbance in the red, as this might bathochromically shift the energy of the PS triplet state below that needed to generate singlet oxygen (unless a drug could be designed with small singlet-triplet separation). However, currently used drugs and silver or gold nanospheres could potentially be employed for PDT in deeper tissues through the use of a red pulsed laser doubled at the cancer location [41] to provide the visible light needed to excite the drug-nanoparticle complexes in the tumor.

In short, we have used the photo-enhancement properties of plasmonic nanoparticles to concentrate the exciting light locally, allowing for a reduction in the amount of PS drug needed for PDT. The ability of plasmonic nanoparticles to enhance the singlet oxygen generation of this model PS drug is greatly dependent on the extent of spectral overlap between the drug absorption and the NP plasmon resonance band. These important concepts will be essential to the design and use of NP conjugates as platforms for the delivery and enhancement of PS drugs in cancer treatment applications.

Author contributions

SCH, LAA, MAE designed research; SCH, LAA performed research; RDN performed theoretical calculations; RO contributed new reagents/reactions; SCH wrote the paper.

The authors declare no conflict of interest.

Acknowledgements

Funding for this work provided by: Georgia Institute of Technology Foundation, the Julius Brown Chair Fund, and the National Institutes of Health Grant NIH-NCI (U01CA151802-01). The authors thank Dr. Paul Szymanski for invaluable help with instrumentation and discussions. Thanks to Z. Hayden, N. Pasqualliero, V. Nguyen, and C. Park for help with synthesis and characterization and to N. Haase for help with DLS measurements. R.O. thanks the Scientific and Technological Research Council of Turkey (TÜBİTAK).

Appendix A. Supplementary data

Supplementary data associated with this article can be found, in the online version, at http://dx.doi.org/10.1016/j.jphotochem.2013.06.004.

References

[1] C. Hopper, Photodynamic therapy: a clinical reality in the treatment of cancer, The lancet oncology 1 (2000) 212–221.
[2] C.K.b. Alexander, Photodynamic therapy, Medical Laser Application, 20 (2005).
[3] K. Kalka, H. Merk, H. Mukhtar, Photodynamic therapy in dermatology, Journal of the American Academy of Dermatology 42 (2000) 389.
[4] E.F. Silva, C. Serpa, J. Dabrowski, C. Monteiro, S. Formosinho, G. Stochel, K. Urbanska, S. Simões, M. Pereira, L. Arnaut, Mechanisms of singlet-oxygen and superoxide-ion generation by porphyrins and bacteriochlorins and their implications in photodynamic therapy, Chemistry (Weinheim an der Bergstrasse Germany) 16 (2010) 9273–9359.
[5] B.W. Henderson, T.J. Dougherty, How does photodynamic therapy work? Photochemistry and Photobiology 55 (1992) 145–157.
[6] M.C. DeRosa, R.J. Crutchley, Photosensitized singlet oxygen and its applications, Coordination Chemistry Reviews 233–234 (2002) 351–371.
[7] C.B. Burger, G.G. Goerres, S.S. Schoenes, A.B. Buck, A.L. Lonn, G.v.S. von Schulthess, PET attenuation coefficients from CT images: experimental evaluation of the transformation of CT into PET 511-keV attenuation coefficients, European Journal of Nuclear Medicine and Molecular Imaging 29 (2002) 922–927.
[8] E.W. Jeffes, J.L. McCullough, G.D. Weinstein, R. Kaplan, S.D. Glazer, J.R. Taylor, Photodynamic therapy of actinic keratoses with topical aminolevulinic acid hydrochloride and fluorescent blue light, Journal of the American Academy of Dermatology 45 (2001) 96–104.
[9] T.J. Dougherty, J.E. Kaufman, A. Goldfarb, K.R. Weishaupt, D. Boyle, A. Mittleman, Photoradiation therapy for the treatment of malignant tumors, Cancer Research 38 (1978) 2628–2635.
[10] D. Dolmans, D. Fukumura, R.K. Jain, Photodynamic therapy for cancer, Nature Reviews Cancer 3 (2003) 380–387.
[11] T. Nyokong, Desired properties of new phthalocyanines for photodynamic therapy, Pure and Applied Chemistry 83 (2011).
[12] R. Lubart, R. Lavie, H. Friedman, The penetration of white light through human tissue, Photomedicine and Laser Surgery 23 (2005) 435–436.
[13] D. Bechet, P. Couleaud, C. Frochot, M.-L. Viriot, F. Guillemin, M. Barberi-Heyob, Nanoparticles as vehicles for delivery of photodynamic therapy agents, Trends in Biotechnology 26 (2008) 612–633.
[14] Y. Cheng, A.C.J. Meyers, Highly efficient drug delivery with gold nanoparticle vectors for in vivo photodynamic therapy of cancer, Journal of the American Chemical Society (2008).
[15] D. Chatterjee, L. Fong, Y. Zhang, Nanoparticles in photodynamic therapy: an emerging paradigm, Advanced drug delivery reviews 60 (2008) 1627–1664.
[16] Y. Fu, J. Zhang, J. Lakowicz, Plasmonic enhancement of single-molecule fluorescence near a silver nanoparticle, Journal of Fluorescence 17 (2007) 811–817.
[17] M.-C. Daniel, D. Astruc, Gold nanoparticles: assembly, supramolecular chemistry, quantum-size-related properties, and applications toward biology, catalysis, and nanotechnology, Chemical Reviews 104 (2004) 293–639.
[18] P.K. Jain, X.H. Huang, I.H. El-Sayed, M.A. El-Sayed, Noble metals on the nanoscale: optical and photothermal properties and some applications in imaging, sensing, biology, and medicine, Accounts of Chemical Research 41 (2008) 1578–1586.
[19] P.K. Jain, K.S. Lee, I.H. El-Sayed, M.A. El-Sayed, Calculated absorption and scattering properties of gold nanoparticles of different size, shape, and composition: applications in biological imaging and biomedicine, Journal of Physical Chemistry B 110 (2006) 7238–7248.
[20] R.L. Phillips, O.R. Miranda, C.C. You, V.M. Rotello, U.H.F. Bunz, Rapid and efficient identification of bacteria using gold-nanoparticle – Poly(para-phenyleneethynylene) constructs, Angewandte Chemie International Edition 47 (2008) 2590–2594.
[21] K.E. Sapsford, L. Berti, I.L. Medintz, Materials for fluorescence resonance energy transfer analysis: beyond traditional donor–acceptor combinations, Angewandte Chemie International Edition 45 (2006).
[22] S. Ondrej, N. Robert, M. Colette, D.M. Brian, Optimization of nanoparticle size for plasmonic enhancement of fluorescence, Plasmonics 2 (2006).
[23] M. Khaing Oo, Y. Yang, Y. Hu, M. Gomez, H. Du, H. Wang, Gold nanoparticle-enhanced and size-dependent generation of reactive oxygen species from protoporphyrin IX, ACS Nano 6 (2012) 1939–1986.
[24] C.-W. Yen, S.C. Hayden, E.C. Dreaden, P. Szymanski, M.A. El-Sayed, Tailoring Plasmonic, Electrostatic field effects to maximize solar energy conversion by bacteriorhodopsin, the other natural photosynthetic system, Nano Letters 11 (2011) 3821–3826.

[25] C. Burda, X.B. Chen, R. Narayanan, M.A. El-Sayed, Chemistry and properties of nanocrystals of different shapes, Chemical Reviews 105 (2005) 1025–1102.
[26] K.S. Lee, M.A. El-Sayed, Dependence of the enhanced optical scattering efficiency relative to that of absorption for gold metal nanorods on aspect ratio, size, end-cap shape, and medium refractive index, Journal of Physical Chemistry B 109 (2005) 20331–20338.
[27] K.S. Lee, M.A. El-Sayed, Gold and silver nanoparticles in sensing and imaging: sensitivity of plasmon response to size, shape, and metal composition, Journal of Physical Chemistry B 110 (2006) 19220–19225.
[28] S. Link, M.A. El-Sayed, Shape and size dependence of radiative, non-radiative and photothermal properties of gold nanocrystals, International Reviews in Physical Chemistry 19 (2000) 409–453.
[29] Y. Chen, K. Munechika, D. Ginger, Dependence of fluorescence intensity on the spectral overlap between fluorophores and plasmon resonant single silver nanoparticles, Nano Letters 7 (2007) 690–696.
[30] B. Nikoobakht, M.A. El-Sayed, Preparation and growth mechanism of gold nanorods (NRs) using seed-mediated growth method, Chemistry of Materials 15 (2003) 1957–1962.
[31] P.J. Flatau, G.L. Stephens, B.T. Draine, Light-scattering by rectangular solids in the discrete-dipole approximation – a new algorithm exploiting the block-toeplitz structure, Journal of the Optical Society of America A Optics, Image Science, and Vision 7 (1990) 593–600.
[32] P.B. Johnson, R.W. Christy, Optical constants of noble metals, Physical Review B 6 (1972) 4370–4379.
[33] E. Hao, G.C. Schatz, Electromagnetic fields around silver nanoparticles and dimers, Journal of Chemical Physics 120 (2004) 357–366.
[34] K.L. Kelly, A.A. Lazarides, G.C. Schatz, Computational electromagnetics of metal nanoparticles and their aggregates, Computing in Science and Engineering 3 (2001) 67–73.
[35] B. Jang, J.-Y. Park, C.-H. Tung, I.-H. Kim, Y. Choi, Gold nanorod-photosensitizer complex for near-infrared fluorescence imaging and photodynamic/photothermal therapy in vivo, ACS Nano 5 (2011) 1086–1180.
[36] A. Tuchscherer, D. Schaarschmidt, S. Schulze, M. Hietschold, H. Lang, Gold nanoparticles generated by thermolysis of all-in-one gold(I) carboxylate complexes, Dalton Transactions 41 (2012) 2738–2746.
[37] A. Grodzicki, I. Łakomska, P. Piszczek, I. Szymańska, E. Szłyk, Copper(I), silver(I) and gold(I) carboxylate complexes as precursors in chemical vapour deposition of thin metallic films, Coordination Chemistry Reviews 249 (2005) 2232–2258.
[38] K. Kuželová, D. Grebeňová, M. Pluskalová, I. Marinov, Z. Hrkal, Early apoptotic features of K562 cell death induced by 5-aminolaevulinic acid-based photodynamic therapy, Journal of Photochemistry and Photobiology B: Biology 73 (2004) 67–78.
[39] L. Austin, B. Kang, C.-W. Yen, M. El-Sayed, Nuclear targeted silver nanospheres perturb the cancer cell cycle differently than those of nanogold, Bioconjugate Chemistry 22 (2011) 2324–2355.
[40] S. Jockusch, N.J. Turro, E.K. Thompson, M. Gouterman, J.B. Callis, G.E. Khalil, Singlet molecular oxygen by direct excitation, Photochemical & Photobiological Sciences 7 (2008) 235–239.
[41] C. Wang, H. Tao, L. Cheng, Z. Liu, Near-infrared light induced in vivo photodynamic therapy of cancer based on upconversion nanoparticles, Biomaterials 32 (2011) 6145–6154.